8th Biennial International Conference
& Exposition on Petroleum Geophysics

"HYDERABAD 2010"

P-75

3-D tomographic Q inversion for compensating frequency dependent attenuation and dispersion

Kefeng Xin* and Barry Hung, *CGGVeritas*

Summary

Following our previous work on Amplitude Tomography that deals with amplitudes alone, we extend our effort to include the compensation of bandwidth and phase of seismic signals that are distorted by seismic attenuation. Our new approach involves utilizing tomographic inversion for estimating the quality factor (Q) from prestack depth migrated common image gathers. By filtering the seismic data into different frequency bands and measuring the effect of attenuation on amplitudes in each band, the frequency dependent effect, which was ignored in our previous work, of attenuation is fully taken into account, allowing Q to be estimated from our tomographic method. By using the estimated Q volume in one of the migration methods that incorporates Q in the traveltime computation, we demonstrate, through examples, that our workflow provides an optimal compensation solution that resolves amplitude and bandwidth distortions due to seismic attenuation.

Introduction

The propagation of seismic wave through viscoacoustic media is affected by the attenuation that is caused by the quality factor Q, resulting in significant loss of signal strength and bandwidth. Gas trapped in sediment is an example of these media. Seismic images of geological structures underneath shallow gas often suffer from resolution degradation and the effect of amplitude dimming, making their identification and interpretation difficult. This in turn affects the ability to accurately predict reservoir properties (Best *et al.*, 1994). Thus, there is a need to compensate the attenuation due to Q.

Complete Q compensation involves the estimation of Q and then using the resultant Q volume to correct the amplitude and phase effects. For the estimation part, various approaches have been utilized. These include the use of VSP data (Ma *et al.*, 2004), crosswell seismic data (Carrillo *et al.*, 2007), and surface seismic data, to name a few. Since the former two types of data are not always available because of the cost reason, seismic surface data are often used for estimating Q and spectral ratio approach is one of the widely used methods for this matter. However, this approach does not take any ray path information into account. For ray based methods such as tomography, amplitude has been used for estimating Q for near surface (Bregman *et al.*, 1989) and on time migrated data (Watanabe and Sassa, 1996). However, these approaches do not consider the actual structures of deeper attenuation anomalies. Frequency information in terms of frequency shift has also been used for estimating Q (Quan and Harris, 1997). Nevertheless, the method is rather sensitive to small frequency changes.

In this paper, we present a ray based tomographic method that is derived from our previous work on amplitude tomography (Hung *et al.*, 2008) for estimating Q. The method is not restricted to attenuation anomalies that are originated from near surface. It takes into account the actual dips of the anomalies because the analysis is performed on the depth migrated data. It overcomes the limitation of our previous work that it compensates only the loss in amplitude. We then demonstrate, with synthetic and real data examples, how we include the estimated Q volume in the depth migration process to fully account for attenuation and dispersion.

Method

Following the steps that are outlined by Hung *et al.* (2008), absorption coefficient β can be obtained by back-projecting amplitude variations from 3D prestack depth migrated data along the traced raypaths and then minimizing the amplitude discrepancies in the common image gathers

(CIGs). The mathematical basis behind the implementation can be expressed as:

$$\ln(\frac{A_o}{A}) = \beta \cdot l \qquad (1)$$

where A_o is the reference amplitude of a particular event, A is the amplitude of the same event that is affected by attenuation at certain locations, l is the distance travelled by the rays through the anomalies and β is given by:

$$\beta = \frac{\pi f}{Qv} \qquad (2)$$

where f is the frequency, v is the velocity and Q is the quality factor representing attenuation. Although attenuation coefficient is a function of frequency, in the frequency range of the seismic wave, Q can be considered to be independent of frequency (Kjartansson, 1979). Hence, the high frequency component of a seismic wave suffers higher attenuation as it propagates in viscoacoustic media.

Using a gridded model in the tomographic inversion process, equations (1) and (2) can be rewritten as:

$$Q_{ijk} = \frac{\pi f_{ijk} l_{ijk}}{\ln(A_o / A_{ijk}) v_{ijk}} \qquad (3)$$

where the index *ijk* respresents a particular 3D gridded cell. Including all the offsets and picked horizons of the CIGs, the tomographic inversion equation for Q update can be described as:

$$\mathbf{F\ m = a} \qquad (4)$$

where **F** is the Frechet derivative matrix, **m** is the vector of attenuation perturbations that involve Q and **a** is the vector containing the logarithmic amplitude ratios. With appropriate preconditioning in the data and model space (Guo *et al*, 2002), the vector **m,** and hence Q, can be solved by standard methods such as least-squares conjugate gradient method.

In terms of the implementation, the steps can be summarized by Figure 1 in which a 3D offset volume of certain frequency is shown. Assuming a horizon has been picked, an amplitude ratio map can be generated along the horizon using a reference average amplitude that is taken from locations that are not affected by the attenuation anomalies. Rays are then shot from the picked points along the horizon to the surface. As the rays going through the gridded cells, the distance travelled within each cell is recorded. These information from a single picked point form a row in the matrix **F** and an element in vector **a**. Using more picked points, offsets and horizons will add more rows into **F** and more elements into **a,** and help to obtain a stabilized solution of Q from the equation (4). By repeating the process for other frequencies, the frequency dependent effect is incorporated into the inversion equation.

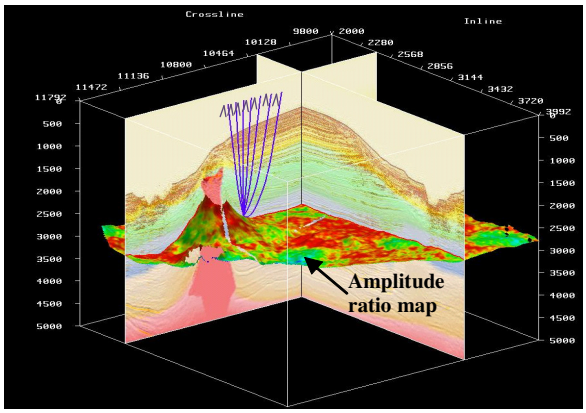

Figure 1. Tomographic scheme for Q inversion.

The resulting Q volume can then be used for mitigating the attenuation effects on amplitude, frequency and phase of the affected seismic signal. Since the correction should ideally be done within the migration process, Q can be used in the computation of complex traveltime (Keers *et al.*, 2001) for ray-based migration methods such as Beam (Gray, 2002) or Kirchhoff migration:

$$T_c(\mathbf{x}) = T(\mathbf{x}) - \frac{1}{2} i \int_{\mathbf{ray}} \frac{1}{c_0 Q} ds - \frac{1}{\pi} \ln(\omega / \omega_0) \int_{\mathbf{ray}} \frac{1}{c_0 Q} ds \qquad (5)$$

where $T(\mathbf{x})$ is the traveltime in the corresponding acoustic medium with velocity c_0 and ω_0 is a reference frequency. Using $T_c(\mathbf{x})$ in our prestack depth migration code (Xie, 2009), the restoration of amplitude and bandwidth can then be demonstrated.

Examples

A synthetic test was first carried out to verify our approach. Figure 2 displays one subline of the 3D model that was used in the test. Five flat events with different reflectivities are present in the model with four localized anomalous

bodies of attenuation with different values of Q are embedded in a non-attenuated background. The losses are constant along the subline direction. Figure 3 shows one of the near offsets of the seismic data that is affected by the anomalous attenuation bodies. The amplitudes of the events are clearly attenuated. Moreover, by extracting five locations (labeled A to E in the figure) for detailed examination, Figure 4 depicts the frequency dependent effect of the attenuation as the shape of the wavelets is distorted.

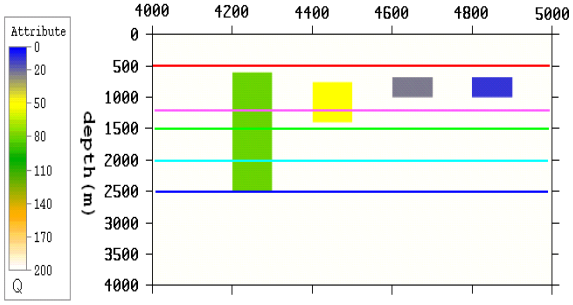

Figure 2. One subline of the 3D model used in the synthetic test. Five flat events are present in the model. Four anomalous Q bodies, which have constant values along the inline direction, are embedded in the non-attenuated background.

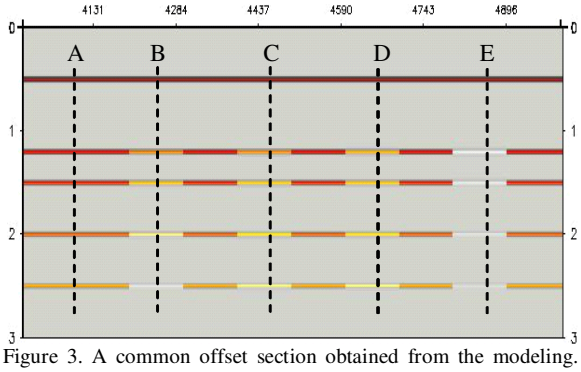

Figure 3. A common offset section obtained from the modeling. Five locations are chosen for detailed wavelets examination.

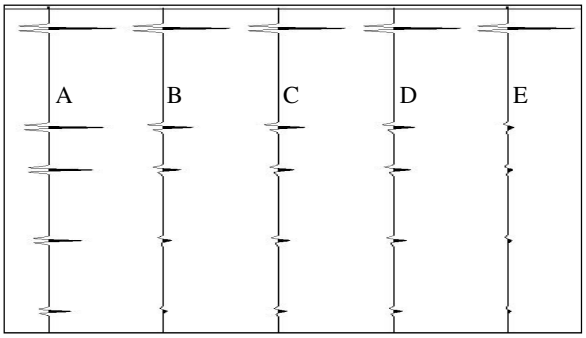

Figure 4. Distortion of the wavelets resulted from frequency dependent attenuation.

The data was then migrated with an amplitude preserving algorithm to ensure that other factors, such as geometrical spreading, that can affect the amplitudes were well handled. By decomposing the migration result into different frequency bands, the amplitude ratios can then be measured along the picked horizons for each band. Figure 5 shows the changes of the amplitude ratio of the fourth event with respect to frequency. As predicted by the theory, the ratios become smaller as the frequency goes higher. Repeating the process for other offsets and then carrying out our tomographic inversion, we obtained a 3D volume of estimated Q anomalies. Figure 6 displays one subline of the estimated Q volume. It can be observed that, apart from the boundary effects that are related to the size of the cells used in the calculation, the Q anomalies are well reconstructed. The estimated Q volume can then be used to correct the attenuation. Figure 7 shows the Q migration result using the method described by Xie (2009). Apart from the migration smiles that are due to the abruptness of our model, the amplitude and bandwidth of the events are well compensated. This can be confirmed by the display of the wavelets shown in Figure 8. Using the location A as the reference as it is not affected by any attenuation, it can be observed that the wavelets of the events at the other four locations match very well with those at the location A.

A real data set on which a zero-offset VSP had been performed was then used for Q estimation using our tomographic method on the surface seismic data. The downgoing waveform in VSP is an ideal dataset for the study of seismic attenuation as it provides a direct observation of how the seismic source wavelet changes with the distance as it propagates (Ma *et al.*, 2004). Figure

9 depicts one of the common offset volumes of the dataset's surface seismic. Five horizons were picked and the amplitude ratios along these events were calculated. As an example, the amplitude ratio map of the fifth event was displayed. Following the procedures that were mentioned above, an interval Q volume was obtained. Extracting the values from the location where the VSP was performed and then converting the interval values to the cumulative values (for the sake of comparison with the given Q values from the VSP), the Q values obtained from the surface seismic are plotted as the red colored curve in Figure 10. In the same graph, the blue colored curve shows the cumulative Q values that were obtained from the VSP through the spectral ratio method. The two sets of values match well with each other, showing that our tomographic method can give a reliable estimation of Q from surface seismic data.

Another data set was tested to show the effect of Q compensation on the migrated result. Figure 11 displays the Q volume estimated from the surface seismic data following the above-mentioned procedures. The values were then used in our Q migration process. Figure 12 depicts a portion of the Q migration result. Comparing this with conventional migration without Q correction that is shown in Figure 13, it can be observed that the Q migration result improves both the resolution and the amplitude fidelity of reflectors below the attenuation anomalies. This can further be confirmed by the amplitude spectra of the two results displayed in Figure 14 which clearly shows that the Q migration result mitigates the amplitude loss in a frequency dependent manner with higher gains experienced by higher frequency components.

Conclusions

We have developed and demonstrated an inversion method based on a post-migration common-image-gather tomography for Q estimation. Synthetic and real data results show that our method can be used to compensate for the amplitude and bandwidth loss associated with attenuation anomalies that can originate from anywhere within the overburden.

References

Best A. I., McCann C. and Sothcott J., 1994, The relationships between the velocities, attenuations and petrophysical properties of reservoir sedimentary rocks: *Geophys. Prosp.*, **42**, 151-178.

Bregman N. D., Chapman C. H. and Bailey R. C., 1989, Travel time and amplitude analysis in seismic tomography: *J. Geophys. Res.*, **94**, 7577-7587.

Carrillo P. and Aldana M., 2007, Attenuation coefficient tomogram and Q distribution image from crosswell survey in the Northern Reef Trend of Michigan Basin: *79th Meeting, SEG*, Expanded Abstracts, 1252-1256.

Gray S., C. Notfors and Bleistein, 2002, Imaging using multi-arrivals: Gaussian beams or multi-arrival Kirchhoff?: *74th Meeting, SEG*, Expanded Abstracts, 1117-1120.

Guo J., Zhou H., Young J. and Gray S., 2002, Toward accurate velocity. models by 3D tomographic velocity analysis: *64th Meeting, EAGE*, B024.

Hung B., Xin K. F., Birdus S. and Sun J., 2008, 3-D Tomographic amplitude inversion for compensating transmission losses in the overburden: *70th Meeting, EAGE*, H004

Keers H., Vasco D. W., and Johnson L. R., 2001,Viscoacoustic crosswell imaging using asymptotic waveforms: *Geophysics*, **66**, 861-870.

Kjartansson E., 1979. Constant Q-wave propagation and attenuation: *J.Geophys. Res.* **82**, 4737-4748.

Ma X. Q., Mouici S., Messaoud M. A. and Djebbar Z., 2004. Q estimation from VSP and surface seismic and its application to improve seismic resolution: *66th Meeting, EAGE*, P003.

Quan Y. and Harris J. M., 1997, Seismic attenuation tomography using the frequency shift method: *Geophysics*, **62**, 895-905.

Watanabe T. and Sassa K., 1996, Seismic Attenuation Tomography and its Application to Rock Mass Evaluation: In. J. Rock Mech. Min. Sci. & Geomech. Abstr., **33**, 467-477.

Xie Y., Xin K. F., Sun J. and Notfors C., 2009. 3D prestack depth migration with compensation for frequency dependent absorption and dispersion: submitted to *79th Meeting, SEG.*

Acknowledgments

We thank Murphy Oil Corp. and OMV for providing us with the data and CGGVeritas for the permission to publish this work.

\

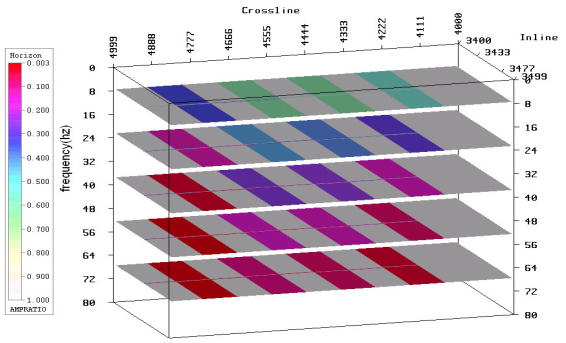

Figure 5. The amplitude ratios of the fourth event measured at different frequencies.

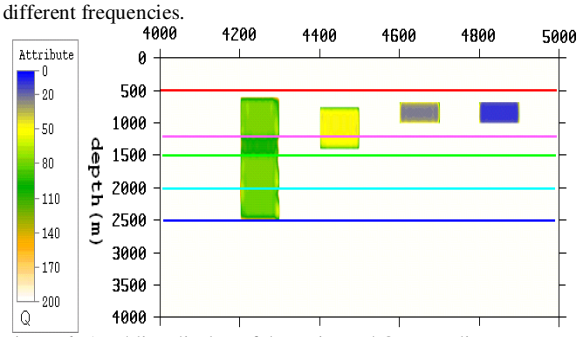

Figure 6. A subline display of the estimated Q anomalies.

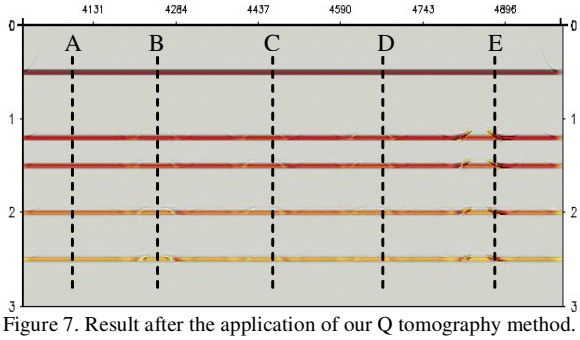

Figure 7. Result after the application of our Q tomography method.

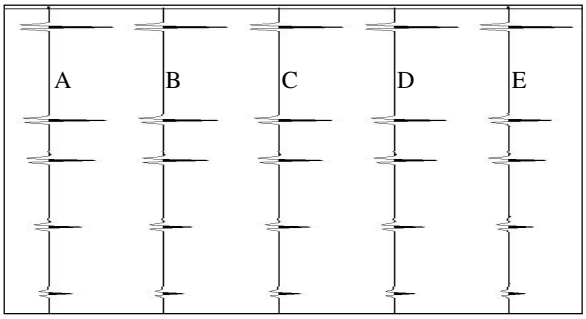

Figure 8. Detailed examination of the wavelets showing restoration of the amplitude and bandwidth after Q migration.

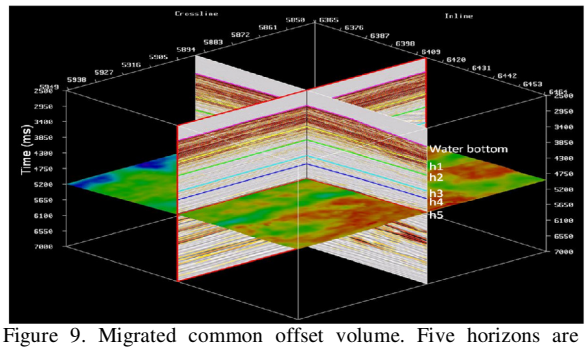

Figure 9. Migrated common offset volume. Five horizons are picked for inversion. The amplitude ratio map of the fifth event is shown. Data courtesy of Murphy Oil Corp.

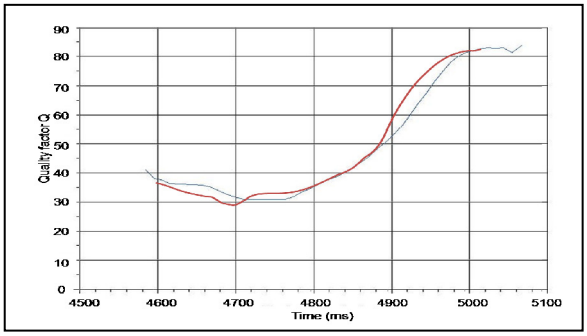

Figure 10. Comparison of the Q values. The blue curve is obtained by the VSP measurement. The red curve is obtained from our tomographic method on the surface seismic data.

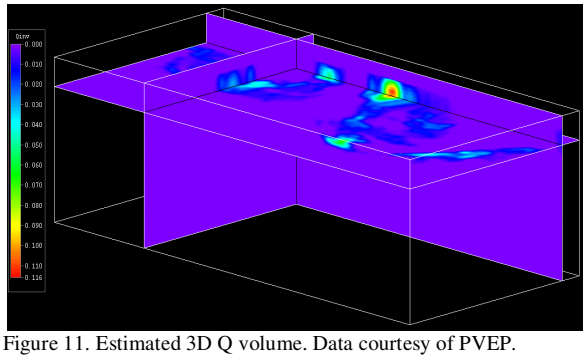

Figure 11. Estimated 3D Q volume. Data courtesy of PVEP.

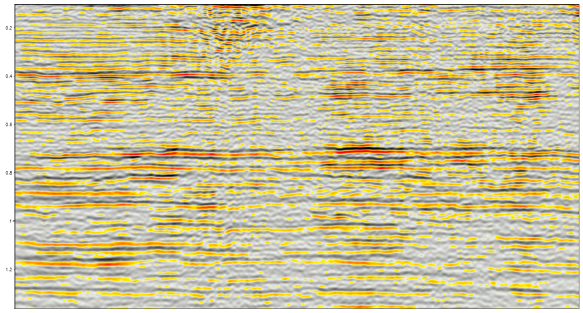

Figure 12. Q compensation result.

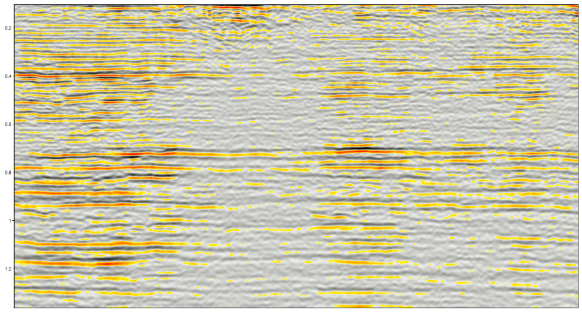

Figure 13. Conventional migration result.

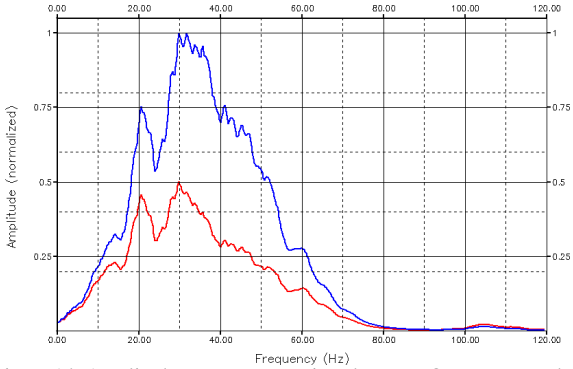

Figure 14. Amplitude spectra comparison between Q compensated (blue) and uncompensated(red) migration results.